applied sciences

MDPI

Article

Role B_4C Addition on Microstructure, Mechanical, and Wear Characteristics of Al-20%Mg_2Si Hybrid Metal Matrix Composite

Hamidreza Ghandvar [1], Mostafa Abbas Jabbar [2], Seyed Saeid Rahimian Koloor [3], Michal Petrů [4], Abdollah Bahador [5], Tuty Asma Abu Bakar [1,*] and Katsuyoshi Kondoh [5]

1 Department of Materials, Manufacturing and Industrial Engineering, Faculty of Engineering, School of Mechanical Engineering, Universiti Teknologi Malaysia, Skudai, Johor Bahru 81310, Malaysia; ghandvar@utm.my
2 Department of Mechanical Techniques, Al-Nasiriya Technical Institute, Southern Technical University, Thi-Qar, Al-Nasiriya 64001, Iraq; m.jabbar@stu.edu.iq
3 Institute for Nanomaterials, Advanced Technologies and Innovation (CXI), Technical University of Liberec (TUL), Studentska 2, 461 17 Liberec, Czech Republic; s.s.r.koloor@gmail.com
4 Technical University of Liberec (TUL), Studentska 2, 461 17 Liberec, Czech Republic; michal.petru@tul.cz
5 JWRI, Osaka University, 11-1 Mihogaoka, Ibaraki, Osaka 567-0047, Japan; abdollah@jwri.osaka-u.ac.jp (A.B.); kondoh@jwri.osaka-u.ac.jp (K.K.)
* Correspondence: tuty@utm.my; Tel.: +60-75534103

Abstract: In the current study, the effect of different B_4C additions (0, 2.5, 5, and 10 wt%) on the microstructural, solidification behavior, mechanical, and tribological properties of Al-20%Mg_2Si composite were studied by means of scanning electron microscopy (SEM) equipped with energy dispersive spectroscopy (EDS), X-ray diffraction (XRD), Vickers hardness, tensile, and dry sliding wear tests. The cooling curve thermal analysis (CCTA) approach was utilized to monitor the influence of B_4C particles on the solidification behavior of Al-20%Mg_2Si composite. The results revealed that the addition of B_4C particles up to 10 wt% reduced the nucleation temperature (T_N) and growth temperature (T_G) of the primary Mg_2Si phase. Moreover, the proper amount of B_4C added to Al-20%Mg_2Si composite has a significant effect on the microstructural alteration, mechanical, and tribological properties of the composite. The mean size of primary Mg_2Si in Al-Mg_2Si composite was 47 μm, in which with the addition of 5 wt% B_4C, the particle size decreased to 33 μm. The highest UTS (217 MPa) and El% (7%) was achieved in Al-20%Mg_2Si-5%B_4C hybrid composite. The cast Al-20%Mg_2Si composite revealed the brittle mode of fracture with some cleavage characterization, in which with the addition of 5%B_4C, the fracture mode altered to a more ductile fracture. The wear results revealed that the Al-20%Mg_2Si-5%B_4C hybrid composite has the highest wear resistance with the lowest wear rate (0.46 mm^3/Km) and friction coefficient (μ = 0.52) under 20 N applied load compared to other fabricated composites with mild abrasion as the governed wear mechanism.

Keywords: Al hybrid composites; Mg_2Si; B_4C; microstructure; thermal analysis; mechanical properties; wear behavior

Citation: Ghandvar, H.; Jabbar, M.A.; Koloor, S.S.R.; Petrů, M.; Bahador, A.; Bakar, T.A.A.; Kondoh, K. Role B_4C Addition on Microstructure, Mechanical, and Wear Characteristics of Al-20%Mg_2Si Hybrid Metal Matrix Composite. *Appl. Sci.* **2021**, *11*, 3047. https://doi.org/10.3390/app11073047

Academic Editor: Theodore Matikas

Received: 18 February 2021
Accepted: 23 March 2021
Published: 29 March 2021

1. Introduction

In recent years, the focus of materials design has moved towards lightweight, low-cost, and environmentally sustainable. According to this trend, aluminum metal matrix composites (AMMCs) have received considerable attention due to their enhanced properties (low density, brilliant cast ability, excellent mechanical properties, and good wear resistance) and low production cost [1].

Magnesium silicide, Mg_2Si, displays high melting temperature (1085 °C), low density (1.99×10^3 kgm^{-3}), high elastic modulus (120 GPa), high hardness (4.5 GPa), and a low coefficient of thermal expansion (7.5×10^{-6} K^{-1}) [2]. As a result of the outstanding

physical and mechanical properties of the Mg_2Si phase, Al-Mg_2Si or Mg-Mg_2Si composites are desirable candidate materials for aerospace, automobile, and other applications [2]. Nevertheless, owing to low temperature brittleness, machinability, and insufficient wear resistance, the application of Al-Mg_2Si composite is limited.

Among the various ceramic particles, boron carbide (B_4C) particles are one of the most promising reinforcement particles as it exhibits unique physical and mechanical properties such as light-weight armor plates for its ballistic properties, wear-resistant components because of its tribological properties, and as abrasive grit. In addition, boron carbide can also be used as a neutron absorber in nuclear reactors due to the nuclear characteristics associated with its high boron content [3,4]. It has bulk modulus of about 214.8–247 MPa [5,6], low thermal conductivity of 30–42 mK, low density (2.52 g cm^{-3}), high hardness 2900–3580 kg/mm^2 and low CTE of $3.2 \cdot 10^{-6}$ $^{\circ}C^{-1}$ [7,8]. Good chemical stability and bonding characteristics with Al alloys are other reported features of B_4C particles [3]. Hence, the B_4C particles are often used to reinforce Al alloys to fabricate MMCs. Baradeswaran et al. [9] identified the influence of B_4C on the mechanical and tribological behavior of Al 7075 composites. They found increasing hardness of composites compared with the base alloy because of the presence of the increased ceramic phase. The wear resistance of the composites increased with increasing content of B_4C particles, and the wear rate was significantly less for the composite material compared to the matrix alloy. In another study, Lashgari et al. [10] studied the influence of heat treatment on tensile properties and wear behavior of A356-10%B_4C composite. They claimed that in Al-B_4C composite, T6 treatment was a dominant factor on the hardness improvement in comparison with hardness increasing due to the addition of B_4C hard particles. In addition, heat treatment process results in higher strength and wear properties of heat-treated metal matrix composites in comparison with an untreated state. Gudipudi et al. [11] investigated the effect of a novel ultrasonic assisted stir casting on mechanical properties of AA6061-B_4C composites. Based on their findings, individual B_4C distribution and the refinement of microstructure was achieved at 4 wt% B_4C. The improved specific ultimate and compressive strengths at 4 wt% B_4C were observed as 36.32% and 43.92%, whereas specific Vicker's and Brinell hardness as 53.41% and 50.89% respectively. A hybrid composite contains two or more reinforcement materials; in which each of the reinforcements deliver superior properties in the composite. As a result, unique mechanical, physical, and tribological properties exist in the hybrid composites, which are not attainable in other materials. Stir casting is implemented to produce the ex-situ (hybrid) aluminium MMCs due to their simplicity and lower cost compared to other fabrication processes [12]. Moktar et al. [13] reported that with the addition of 10 wt% SiC particles to Al-20%Mg_2Si composite, the morphology of primary Mg_2Si was altered to polygonal and its size decreased to 30 µm. Similarly, Sukiman et al. [14] reported that when the Al-15%Mg_2Si composite was added with 6 wt% YSZ, the mean size of primary Mg_2Si reduced to 72.4 µm with subsequent improvement in tensile properties of the composite. Uvaraja et al. [15] examined the effect of SiC and B_4C particulates-reinforced composite on Al6061 matrix. It was observed that hybrid metal matrix composites (HMMCs) showed a high level of hardness as compared to alloy because silicon carbide and boron carbide particles were uniformly embedded in the Al6061 matrix. Aziz et al. [16] studied the heat treatment and wear properties of Al_2O_3 and TiC particulates in reinforced Al6063 hybrid composites. The hardness of the composites was improved after heat treatment due to the presence of reinforcements in the composite, which accelerated the aging kinetics and caused an increase in dislocation density at the surrounding area of the reinforcement particles. Benal et al. [17] studied the effects of reinforcement with SiC and E-glass fibers on the wear properties of Al6061 hybrid composites. Due to the presence of both hard reinforcements and coherent precipitates in the matrix, increased hardness was observed during aging treatment. Umanath et al. [18] studied the effect of stir casting processing method to prepare Al6061-SiC-Al_2O_3 hybrid composites. It was observed that by adding reinforcement particles to the alloy matrix, micro-hardness increases with increased reinforcement due to solid solution hardening

of the matrix. Altinkok et al. [19] evaluated the tensile behavior and microstructure of Al_2O_3/SiCp-reinforced AMMCs fabricated by the stir casting technique. Strength of the hybrid composite was higher than the unreinforced alloy. The significant enhancement in tensile strength of the composites was attributed to the grain and particle size, reinforcement shape, and uniform particle distribution in the alloy matrix. Uvaraja et al. [20] focused on the tribological behavior of novel hybrid composite materials by varying SiC reinforcements and a fixed percentage of B_4C particles. It was observed that the increase in hardness of the composite was mainly owed to the existence of harder SiC and B_4C particles in the matrix alloy, which act as obstacles to the dislocation motion. Sharma et al. [21] examined the metallography and bulk hardness of artificially aged Al6061-B_4C-SiC stir cast hybrid composites. A significant improvement in hardness, tensile strength, and a marginal decrease in ductility of hybrid composites were observed compared to aluminum alloy. Uthayakumar et al. [22] studied the wear performance of Al1100-SiC-B_4C hybrid composites under dry sliding conditions. An increase in hardness and wear resistance was observed due to the existence of harder SiC and B_4C reinforcement particles in the matrix alloy.

Although there are several studies in the literature on the structure and properties of Al hybrid composites reinforced with B_4C and other particles such as SiC, Al_2O_3, etc.; however, information regarding the structure and properties of Al hybrid composite reinforced with B_4C and Mg_2Si (Al-Mg_2Si-B_4C) is rather limited. Therefore, the purpose of the present study is to elucidate the influence of the different content of B_4C particles on microstructure alteration, solidification behavior, mechanical properties, and wear properties of Al-20%Mg_2Si composite.

2. Materials and Methods

2.1. Materials Fabrication

The initial materials to prepare Al-Mg_2Si-B_4C hybrid composites were pure aluminium (99.9% purity), pure magnesium (99.9% purity), pure silicon (98.9% purity), and pure B_4C ceramic powder with a size of 10–30 μm. In order to fabricate the hybrid composites, Al ingot was melted at 800 °C using an induction furnace, and then Si was added to the molten metal at the same temperature. After dissolving the Si in Al, the melt temperature was reduced to 750 ± 10 °C and pure magnesium was then introduced to the melt. The temperature was reduced to prevent the oxidation of Mg. After homogenization and removal of the dross, the melt was poured into a steel mold to produce the composite ingot. To fabricate the hybrid composites, 2 kg of composite ingot was melted in a resistance furnace and then, B_4C particles (2.5 wt%) were added gradually into the Al-Mg-Si melt. The melt was stirred constantly at a speed of 500 rpm for 15 min at 750 °C to obtain a uniform dispersion of reinforcement particles in the molten metal [23,24]. In fact, due to high viscosity of the composite melt, long stirring time is needed to achieve good mixing of the reinforcement particles inside the melt. The hybrid composite melt was cast in the pre-heated (220 °C) cast iron die to solidify. The procedure was repeated to prepare hybrid composites with 0, 5, and 10 wt% B_4C. The fabricated samples were used for microstructure examination, mechanical tests, and wear tests.

2.2. Cooling Curve Thermal Analysis

Parallel to the casting of the composites, in order to examine the influence of B_4C particles on characteristic temperatures of primary Mg_2Si phase during solidification, thermal analysis was conducted, in which the molten metal was poured into a preheated cylindrical ceramic mold (800 °C for 20 min) which was embedded by a K-type thermocouple located in the middle, 15 mm above the bottom of the mold. The temperature-time data were achieved using EPAD-TH8-K and EPAD-BASE module connected to a computer with DEWESoft 7.0.5. The FlexPro 2019 data analysis software was used to extract the recorded data and smooth and plot the cooling curves, as well as the first and second derivative curves for extracting solidification parameters. For the fabricated composites, the slope of

the cooling curve before nucleation temperature of primary Mg_2Si was used to calculate the cooling rate. The cooling curve calculated for all thermal analysis tests was about 0.7 °C/s.

2.3. Mechanical Tests

The uniaxial tensile test was carried out based on ASTM B557M-02a by a computerized universal testing machine (Instron 5982) equipped with a strain gauge extensometer at a constant cross-head speed of 1 mm/min in room temperature. To confirm repeatability of the results, the tensile test was conducted on at least three specimens for each test. Hardness of the specimens was measured by a Matsuzawa Vickers hardness testing machine with the diamond indenter having an angle of 136° between opposite faces at a load of 5 N with a dwell of about 30 s.

2.4. Sliding Wear Test

Pin-on-disc sliding wear testing machine (TR-20, DUCOM) was utilized to investigate the wear properties of the composites according to the ASTM G99-04a standard under applied loads of 20 and 40 N, at constant parameters of 60 mm track diameter, 200 rpm sliding speed and 2000 m sliding distance, against a hardened chromium steel disc (Rc 64). The pin samples were 25 mm in length and 6 mm in diameter. The height loss of the specimens was measured using a linear variable differential transformer (LVDT) to monitor the wear loss of the specimens in microns. The volumetric loss was calculated by multiplying the height loss with cross section area of the test pin. A frictional force sensor was used to measure the generated frictional force on the specimens in Newton. A set of three samples was tested for each experimental condition and the average values were used for further analysis.

2.5. Microstructure Characterization

For microstructure characterization, the specimens were cut from the middle portion of cast billets and then underwent the grinding and polishing procedures in accordance with the standard metallography routines. Microstructures were analyzed using scanning electron microscopy, SEM (Hitachi S3400N) equipped with EDX facility. The fracture surfaces of the tensile test as well as the worn surface of the wear test specimens were cleaned with acetone using ultrasonic cleanser and examined using SEM. An I-Solution image analyzer was used to calculate the quantitative characteristics of the microstructure density, and aspect ratio as

$$\text{Mean density} = \frac{1}{m}\sum_{j=1}^{m}\left(\frac{1}{n}\sum_{i=1}^{n} D_i\right)_i \quad (1)$$

$$\text{Mean aspect ratio} = \frac{1}{m}\sum_{j=1}^{m}\left(\frac{1}{n}\sum_{i=1}^{n} \frac{a_i}{b_i}\right)_i \quad (2)$$

where D_i, a_i, and b_i are the density, longest, and shortest dimensions of a single Mg_2Si particle respectively, n is the number of Mg_2Si particles measured in a single field (0.60126 mm^2), and m is the number of the evaluated fields. Furthermore, X-ray diffraction (XRD) (PHILIPS binary diffractometer with Cu-kα radiation application) was utilized to analyze the phase constituents of the fabricated hybrid composite.

3. Results and Discussion

3.1. Microstructure Examination

The microstructural micrograph of Al-20%Mg_2Si-10% B_4C hybrid composite is shown in Figure 1a. As seen, the composite structure consists of α-Al as matrix and Mg_2Si and B_4C as reinforcement particles. The corresponding elemental mapping as well as the XRD patterns of Al-20%Mg_2Si-10% B_4C hybrid composite is illustrated in Figures 1b and 2 respectively, which indicate the existence of the Al, Mg_2Si and B_4C in the HMMC.

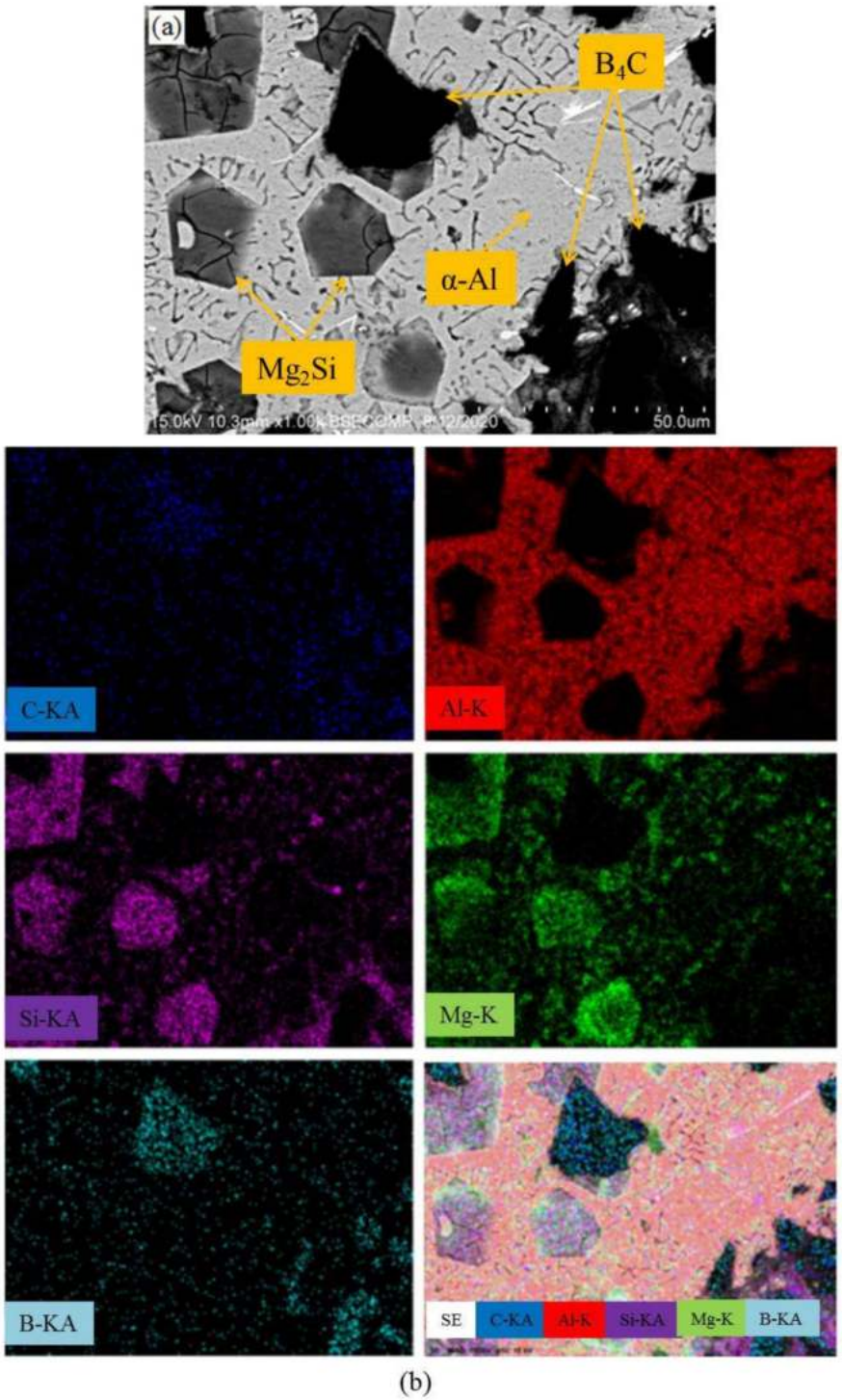

Figure 1. (**a**) SEM image of Al-20%Mg_2Si composite with B_4C addition with (**b**) corresponding elemental mapping analysis.

Figure 3a–d exhibits the SEM micrographs of Al-20%Mg_2Si composite added with different B_4C concentrations. As seen in Figure 3a, in the composite without B_4C particles (base), primary Mg_2Si particles are large and irregular and often in polyhedral shape surrounded with eutectic Mg_2Si cells. With the addition of 2.5 wt% B_4C into the Al-Mg_2Si composite, the morphology of primary Mg_2Si is still in polyhedral shape, as shown in Figure 3b. However, when the composite was treated with 5 wt% B_4C, the morphology of primary Mg_2Si slightly altered to polygonal as depicted in Figure 3c. Moreover, B_4C particles are distributed homogeneously throughout the aluminium matrix. With further

addition of B_4C particles until 10 wt%, the Mg_2Si particles retain the polygonal morphology; however, some agglomeration of B_4C particles are observed in the composite area as illustrated in Figure 3d. Similar behavior of produced agglomeration as a result of increased B_4C reinforcement content in Al composites was reported by other researchers [25–27]. This phenomenon can be attributed to the insignificant wettability of ceramic particles with aluminum melt as the particles float on top of the melt surface owing to the surface tension and high interfacial energy of the reinforcing particles [28]. Besides, the lower density of B_4C particles compared to the aluminum causes the B_4C particles to float and leads to the non-uniformed dispersion where the B_4C particles agglomerate and segregate at a particular place in the melt.

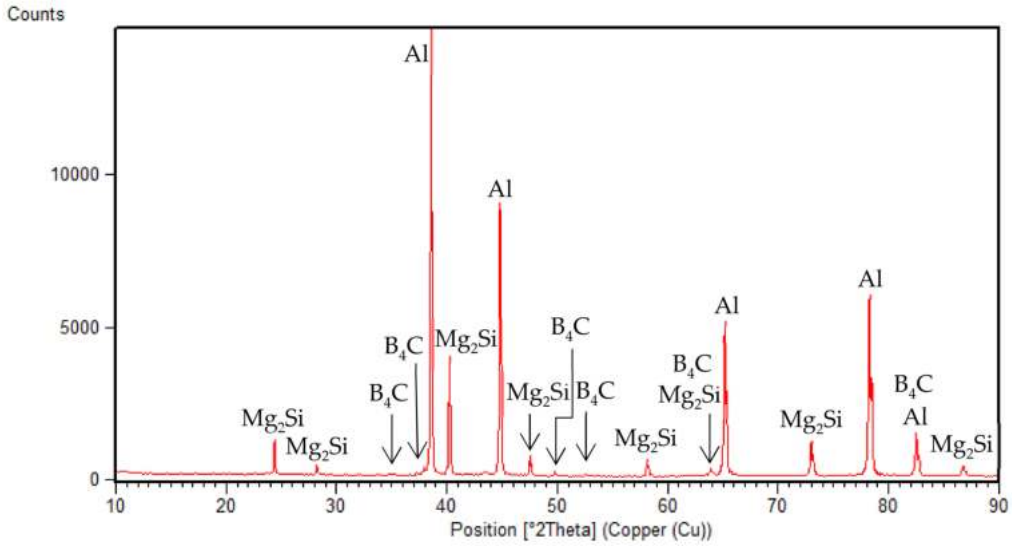

Figure 2. XRD results of Al-20%Mg_2Si in situ composite added with 10 wt. % B_4C.

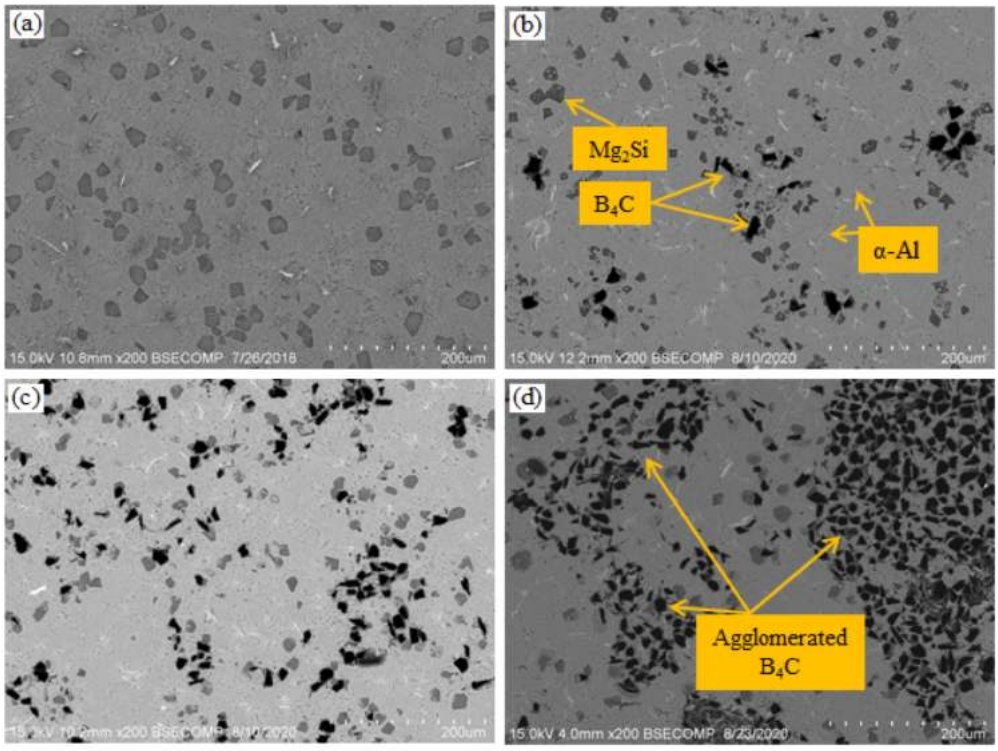

Figure 3. SEM images of Al-20%Mg_2Si composite with various additions of B_4C: (**a**) 0 wt%, (**b**) 2.5 wt %, (**c**) 5 wt%, and (**d**) 10 wt%.

3.2. Quantitative Analysis of Microstructure

Figure 4 shows that the alterations in average particle size, aspect ratio, and particle formation per unit area (density) correspond to the various B_4C additions. The results match well with the microstructure observation in Figure 3, in which with the addition of 2.5 wt% B_4C, the average particle size decreased by 13% from 47 to 41μm, the aspect ratio decreased by 3.7% from 1.34 to 1.29, and the density also decreased by 16% from 135 to 113 particle/mm^2. With the addition of 5 wt% B_4C to Al-20%Mg_2Si composite, the particles size, aspect ratio, and density of primary Mg_2Si further decreased to 33 μm, 1.27 and 94 particle/mm^2. However, as observed in Figure 3, with a further addition of B_4C to 10 wt%, the mean size and aspect ratio of primary Mg_2Si increased to 38 μm and 1.28 respectively. Nevertheless, the density decreased to 63 particle/mm^2 (Figure 4). Therefore, according to the results in Figures 3 and 4, it can be observed that Al-20%Mg_2Si-5%B_4C hybrid composite illustrates the best condition in terms of primary Mg_2Si refinement and B_4C particles distribution.

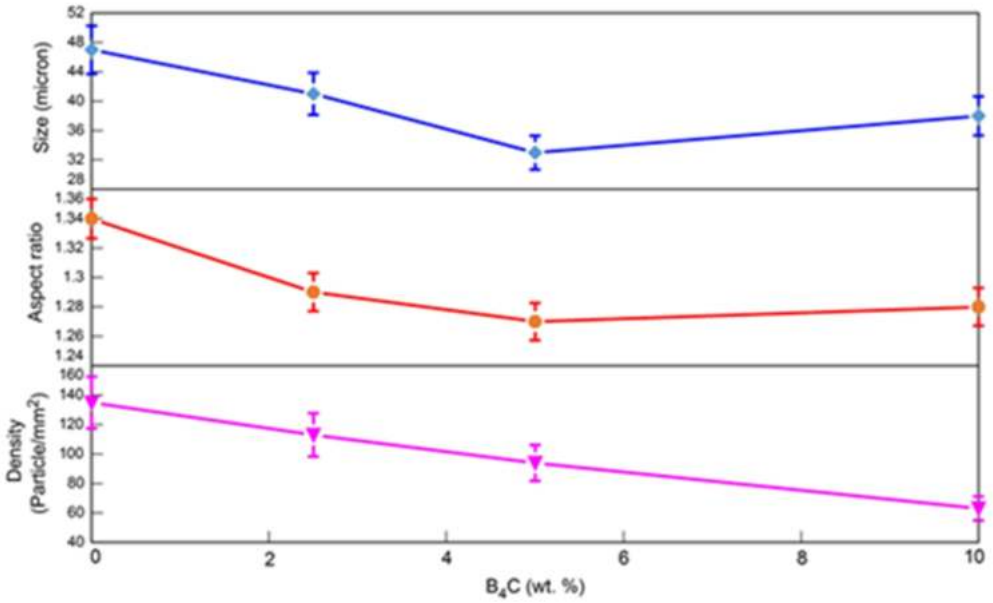

Figure 4. Characteristics of primary Mg_2Si particles in Al-20%Mg_2Si composite treated with various content of B_4C.

3.3. Influence of B_4C Addition on Cooling Curves

Figure 5 demonstrates the cooling curve of Al-20%Mg_2Si composite with the first and second derivative curves corresponds to different contents of B_4C. The peaks on the first and second derivative curves represent distinct phase transformations that occurred during solidification. According to the binary phase diagram of Al-20%Mg_2Si, the first phase is the primary Mg_2Si, while the second phase is the formation of eutectic Al-Mg_2Si. It is observed that the addition of B_4C altered the solidification behavior of the Al-20%Mg_2Si composite by changing the solidification temperatures (nucleation temperature (T_N), growth temperature (T_G)) of primary Mg_2Si phase that is correlated with the microstructures of the composites, as observed in Figure 3.

Figure 6 shows the nucleation temperature (T_N) and growth temperature (T_G) of the primary Mg_2Si phase which correspond to the various additions of B_4C. The plotted graph of T_N has the same pattern as T_G of primary Mg_2Si, representing the same influence of the B_4C on these temperatures. Based on the result, it can be observed that the T_N of primary Mg_2Si decreased when the B_4C addition was introduced from 2.5 to 10 wt%. The same trend of graph is also observed for the T_G of primary Mg_2Si phase. From the temperature of 659.2 °C for base Al-20%Mg_2Si composite, T_N of primary Mg_2Si decreased to 659 °C, 657 °C, and 655.8 °C after the addition of 2.5, 5, and 10 wt% B_4C respectively.

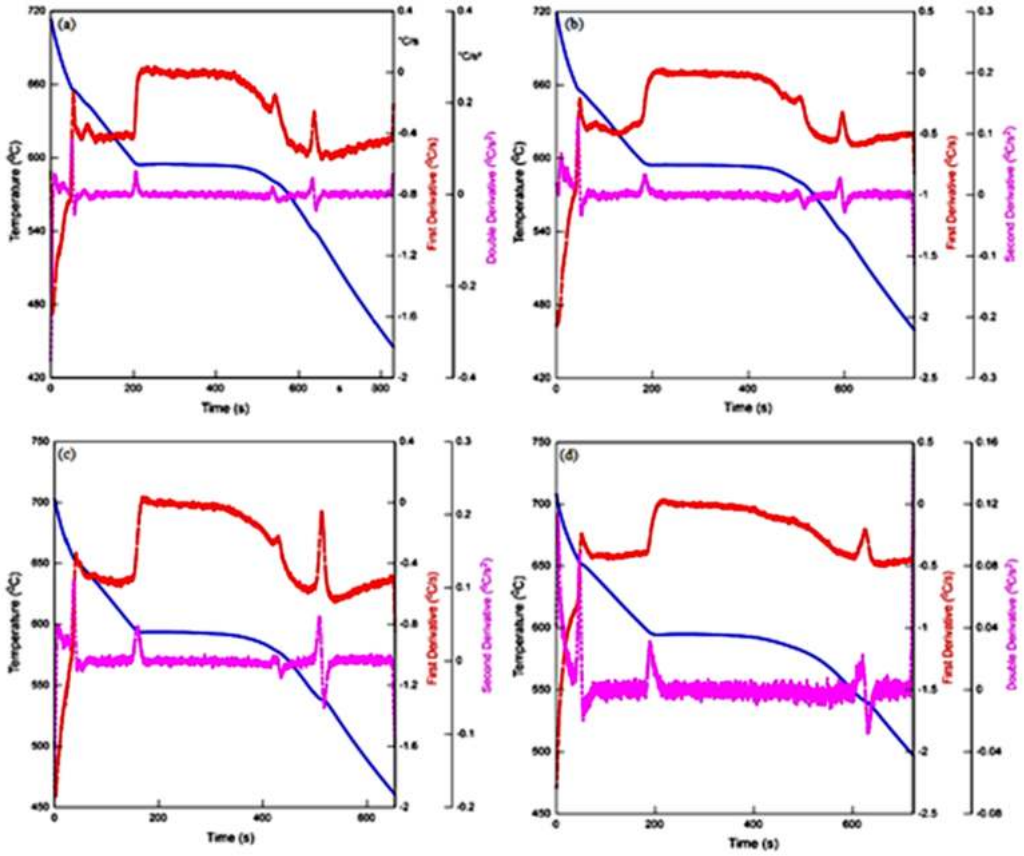

Figure 5. Cooling curves with first and second derivative curves of the Al-20%Mg_2Si composite added with various B_4C concentrations: (**a**) 0, (**b**) 2.5, (**c**) 5, and (**d**)10 wt%.

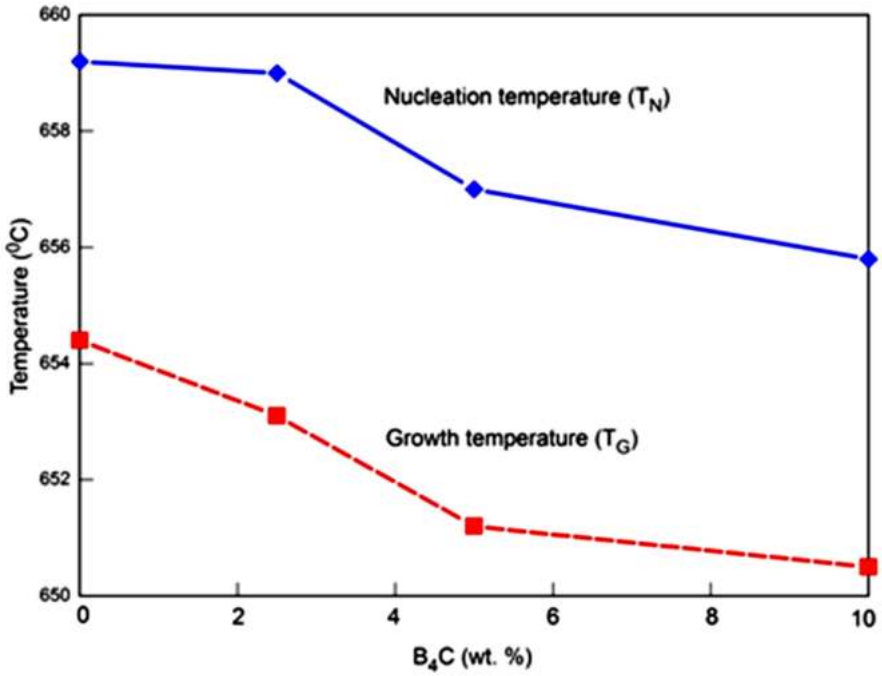

Figure 6. Nucleation temperature (T_N) and growth temperature (T_G) of primary Mg_2Si phase correspond to different B_4C additions.

Figure 7 depicts the duration (Δt) of primary Mg_2Si particles formation. The t_GMg_2Si-t_NMg_2Si is used to indicate the time needed for the primary Mg_2Si to nucleate and grow

until complete solidification before the beginning of the eutectic cells. In the base Al-20%Mg_2Si composite, the duration of primary Mg_2Si to grow is about 13.82 s. The duration is reduced to 12.59 and 10.32 s as the composite was added with 2.5 and 5 wt% B_4C, respectively. Nonetheless, the duration of primary Mg_2Si particles formation increased to 12.42 s when the composite is treated with 10 wt% B_4C. The difference between the duration is small, which is no more than 3.5 s. It is probable that B_4C addition plays a role in controlling the growth of Mg_2Si particles, which results in the changing particle size. The obtained results demonstrate that when Al-20%Mg_2Si composite is added with 5%B_4C particles, the duration of primary Mg_2Si formation is less than other B_4C additions, which is consistent with the results in Figures 3 and 4, in which the addition of 5%B_4C to Al-20%Mg_2Si composite caused the most refinement effect on primary Mg_2Si particles.

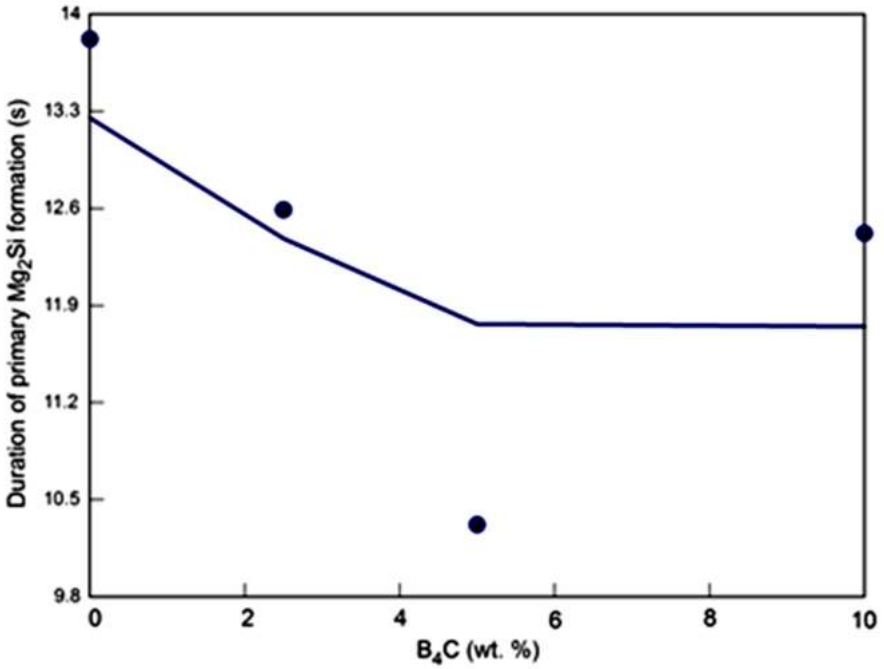

Figure 7. Duration of primary Mg_2Si particles to nucleate and grow as a result of B_4C additions.

3.4. Refinement Mechanism of B_4C Addition

The results obtained from microstructure and thermal analysis clearly demonstrate that addition of B_4C particles to Al-Mg_2Si composite caused partial refinement of the Mg_2Si particles. The appropriate refinement has been obtained with addition of 5 wt% B_4C. Figure 8 illustrates the SEM microgrpah of primary Mg_2Si particles including dark particle in its center with corresponding line scanning spectra analysis. As seen, the EDS analysis reavled that the dark color particle in the centre of primary Mg_2Si is B_4C. The existance of this particle in the center of Mg_2Si crystal propose that B_4C particle may provide favorable nucleation substrates for the Mg_2Si particles precipitation.

In order to find out whether the refining effect is related to the role of B_4C particles as heterogeneous nucleation sites for primary Mg_2Si, the crystal structures of Mg_2Si and B_4C were compared and the lattice misfit between these crystal structures was calculated. The crystal structures of B_4C and Mg_2Si are shown in Figure 9. It can be clearly observed that the atoms distributed on the B_4C and Mg_2Si planes are in a different manner. In addition, the calculated lattice misfit between the B_4C and Mg_2Si is 43.6%. According to Bramfitt's two-dimensional lattice misfit theory, if the mismatch between two planes is below 15%, one phase can act as a heterogeneous nucleation substrate for another [29]. Thus, it is observed that B_4C particles is not likely to meet the character of heterogeneous nucleation substrates for primary Mg_2Si crystals.

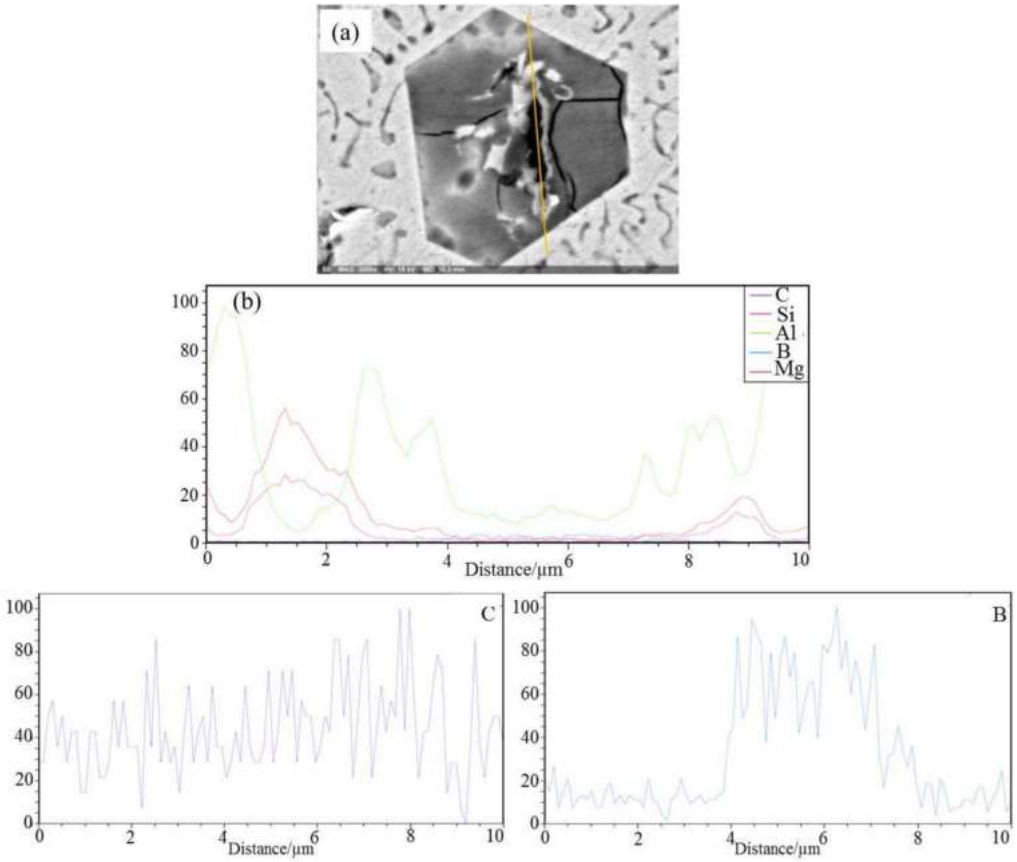

Figure 8. (**a**) SEM micrograph of primary Mg_2Si crystal including B_4C particle, (**b**) corresponding elemental mapping analysis.

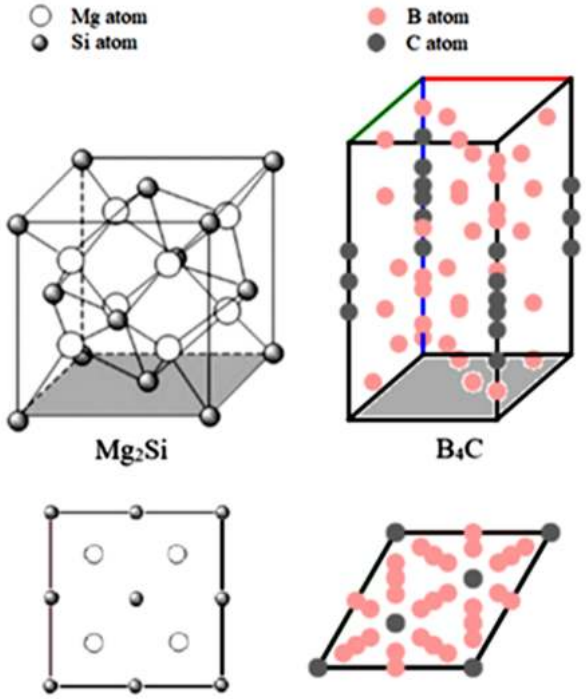

Figure 9. Comparison of crystal structures of Mg_2Si and B_4C crystals.

In addition, Figure 6 depicts that with the addition of B_4C particles to Al-Mg_2Si composite, the nucleation temperature (T_N) of primary Mg_2Si was reduced. It has been reported that provision of heterogeneous nucleation substrates for primary Mg_2Si particles through addition of refiners occurred at higher nucleation temperatures which results in a refined microstructure of the composites [30,31]. Hence, it can be concluded that the refinement of Mg_2Si particles as a result of B_4C addition is related to the growth stage rather than nucleation. The possible reason for refinement of primary Mg_2Si particles is the presence of the B_4C particles that act as a physical barrier during the growth of the primary Mg_2Si phase during solidification. According to the particle pushing phenomenon, the B_4C particles are rejected by the solidification front and finally stuck in grain boundary areas [32].

It was expected that with the addition of higher content of B_4C particles (10 wt%) to Al-20%Mg_2Si composite, the size of the primary Mg_2Si decreases. However, as shown in Figures 3 and 4, addition of 10 wt% B_4C results in a reverse trend as the mean size of primary Mg_2Si particles increased. In fact, in Al-20%Mg_2Si-10%B_4C hybrid composite, the B_4C particles are agglomerated in some areas in the matrix with non-uniform distribution throughout the composite matrix; therefore, they cannot effectively hinder the growth of primary Mg_2Si particles in the preferred Mg_2Si growth directions, which results in an increase in the particles size. Moreover, the average number of primary Mg_2Si particles per unit (mm^2) (density) decreased with the increasing B_4C concentration up to 10 wt%, as illustrated in Figure 3. The drop in the density of primary Mg_2Si particles as a result of B_4C addition can be associated with the formation of some boron-containing compounds in the matrix of the composite. According to Shirvanimoghaddam et al. [25], and Li et al. [33], some B-containing compounds are detected in the various B_4C reinforced aluminium composites, in which some B elements are dissolved from B_4C particles into the liquid-solid interface. As observed in Figure 10, the SEM micrograph with corresponding EDX results depicts that the presence of these boride compounds consist of Al and Mg. The formation of Al-Mg-B consumes the existed Mg in the melt, and hence, the amount of Mg atoms to react with Si to produce Mg_2Si decreased. This findings are aligned with the results by Azarbarmas et al. [34] where 1%B was added to Al-15%Mg_2Si composite. In fact, partial dissolution of B_4C in Al leads to the formation of B-containing compounds. Viala et al. [35] have pointed out that as a result of the reaction between Al and B_4C at temperatures above 700 °C, AlB_2, Al_3BC, and Al_4BC are produced. The dissolution of B_4C immediately saturates the molten Al with carbon and boron since the solubility of these elements in Al is low [36]. However, as the amount of Al-Mg-B phase is small, it is difficult to detect them in the XRD patterns (Figure 2). The observation in the density of primary Mg_2Si particles as a result of increasing B_4C content is consistent with the decreasing trend of nucleation temperature (T_N) of primary Mg_2Si phase in Figure 6. In fact, the reduction of Mg in the melt as a result of the formation of Al-Mg-B compound leads to a shift in the composition of the Al-Mg_2Si composite to lower the Mg_2Si content (eutectic point); hence, the nucleation temperature of primary Mg_2Si phase decreased.

According to Azarbarmas et al. [34], in the Al-Mg_2Si composite treated with B element, beside the segregation of boron on the solid-liquid interface, some B atoms also adsorbed on the growth front and changed the surface energy of the Mg_2Si crystals. Nevertheless, in the present study, due to the interaction of B with the melt and formation of B-rich intermetallic compounds, more B atoms are consumed, in which the extra B atoms are inadequate in the melt to absorb the primary Mg_2Si growth front and poison its anisotropic growth and alter its morphology significantly. Therefore, as shown in Figures 3 and 4, addition of B_4C particles into Al-20%Mg_2Si composite has a minor impact on the aspect ratio of primary Mg_2Si particles, in which the maximum alteration of the aspect ratio occurred after the addition of 5 wt% B_4C (5.22%) compared to the base composite. This result demonstrates that B_4C addition has no obvious changes on the structure of primary Mg_2Si particles.

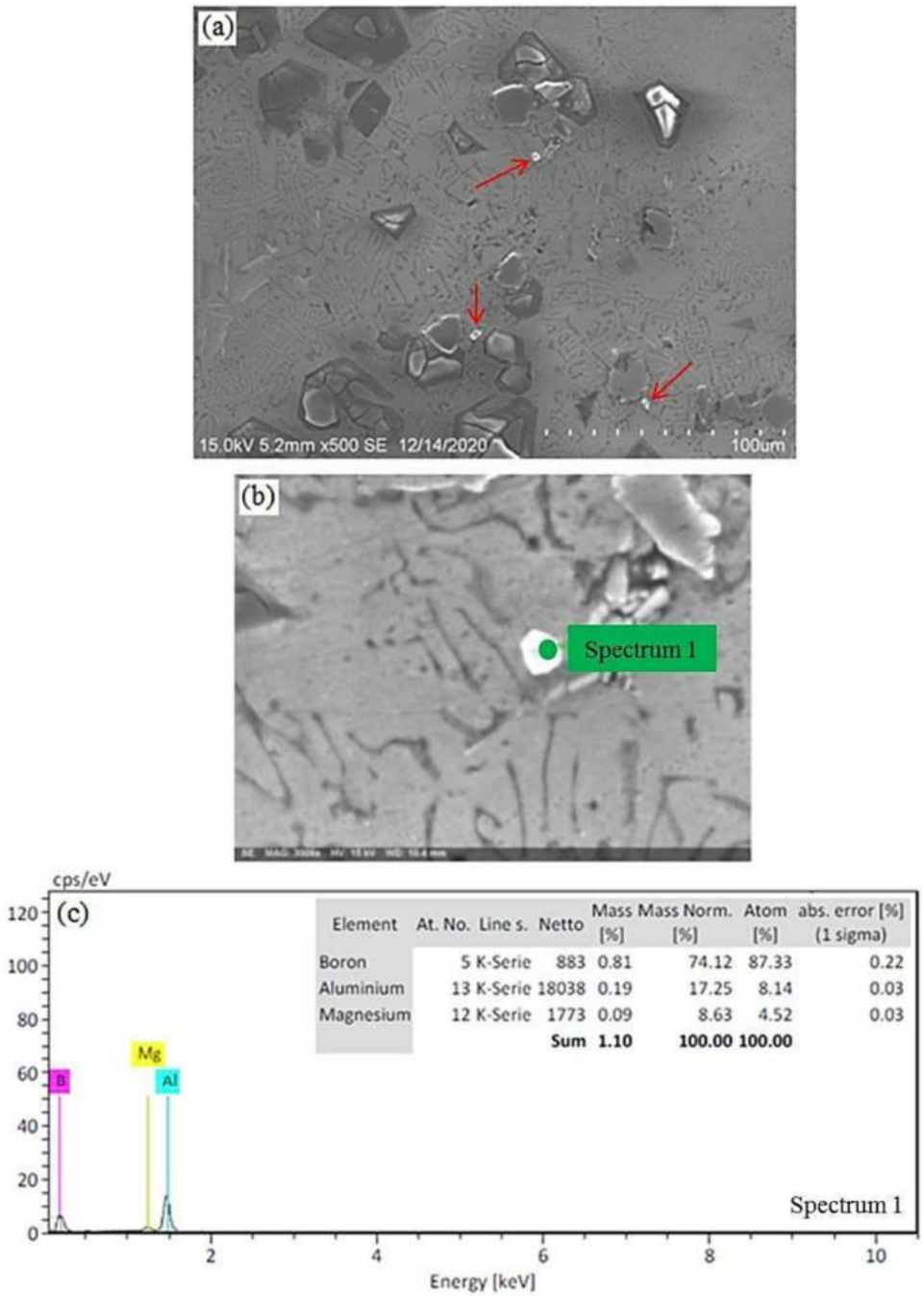

Figure 10. (**a**) BSE micrograph of Al-20%Mg_2Si-10%B_4C hybrid composite, (**b**) SEM image of Al-Mg-B compound, and (**c**) corresponding EDS result of the white particle in (**b**).

3.5. Mechanical Properties

3.5.1. Hardness

The average Vickers hardness of the fabricated composites as a result of different B_4C additions is illustrated in Figure 11. It can be observed that with the addition of 2.5 and 5.0 wt% B_4C ceramic particles to Al-20%Mg_2Si composite, the hardness value increased to 79 and 100 HV, respectively in comparison with the base composite (75 HV). The enhancement in the hardness property is attributed to the refinement of primary Mg_2Si particles as well as increasing the content of B_4C reinforcements. As observed, the hardness value of Al-20%Mg_2Si-5%B_4C hybrid composite is greater than other fabricated composite, which is due to the uniform distribution of B_4C particles. The existence of hard

B_4C and fine Mg_2Si particles increased the obstacles to the grain boundary sliding [37]. Another factor for the improvement of the hardness of the composite due to B_4C addition is increase in the dislocation density as a result of thermal expansion mismatch among the reinforcement and matrix at the particle-matrix interfaces [11]. These factors result in high restrictions to the localized deformation during indentation. However, with further addition of B_4C particles to 10 wt%, the hardness value decreased to 84 HV. The reason for the decreasing hardness value is due to the agglomeration of B_4C particles in the matrix of the composite (Figure 3d). In addition, as depicted in Figure 4, by increasing the B_4C concentration to 10 wt%, the size of primary Mg_2Si particles increased and the density of primary Mg_2Si particles in the composite decreased as well, hence, the number of the Mg_2Si particles to resist the applied load during the hardness test is reduced. Therefore, both B_4C agglomeration and low density of primary Mg_2Si particles cause a higher exposure of the soft aluminium matrix to the intender, and as a result, the average hardness of the composite is reduced.

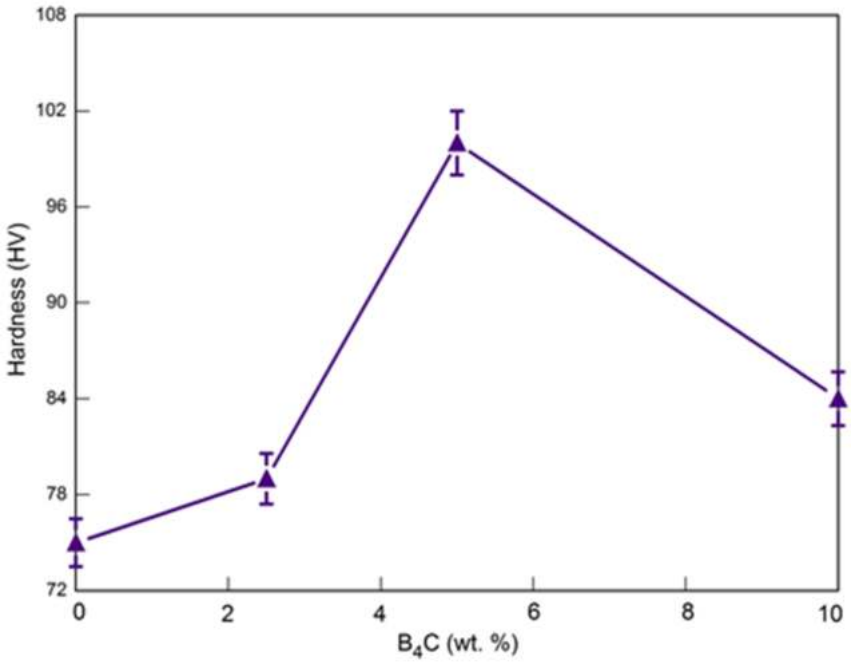

Figure 11. Vickers hardness of Al-20%Mg_2Si composite treated with various amount of B_4C particles.

3.5.2. Tensile Properties

The engineering stress-strain curves of Al-Mg_2Si composite added with various contents of B_4C ceramic particles is illustrated in Figure 12a. The ultimate tensile strength (UTS) and elongation percentage to failure (El%) values of the composites are demonstrated in Figure 12b,c respectively. As seen, the addition of 2.5 and 5 wt% B_4C to Al-20%Mg_2Si composite increased the tensile properties, in which the addition of 5 wt% B_4C results is the highest value as the ultimate tensile strength (UTS) and percentage elongation (El%) increased from 177 MPa and 4.6% in the base Al-20%Mg_2Si composite to 217 MPa and 7% in Al-20%Mg_2Si-5%B_4C hybrid composite. It can be observed that there is a consistency between these results and the microstructural observations in Figure 3 as Al-20%Mg_2Si-5%B_4C hybrid composite exhibits a uniform distribution of B_4C reinforcements as well as refined primary Mg_2Si particles. The high strength values of Al-20%Mg_2Si-5%B_4C hybrid composite is due to the existence of B_4C particles in the composite matrix with uniform distribution, which creates dislocation pile-up in their neighborhood. Thus, the strength of the composite enhanced as a result of increasing dislocation interactions and dislocation density in the matrix near interfaces of the matrix and reinforcement.

In addition, partial refinement of primary Mg_2Si particles has a significant impact on strength enhancement of the composite. As depicted in Figure 3a, in base Al-20%Mg_2Si, the primary Mg_2Si particles exist with polyhedral shape and sharp tips, in which these sharp areas are potential sites for stress concentration which cause a drop in tensile properties. Nevertheless, in Al-20%Mg_2Si-5%B_4C hybrid composite, the primary Mg_2Si particles are finer and their morphology is regular (Figure 3c) compared to the base material, which results in tensile improvement. The most probable explanation of this behavior could be a deformation stregthening of hybrid composites which are brittle in nature but demonstrate higher strength and elongation when added with B_4C particles due to Hall-Petch dependence on the Mg_2Si particles size. The effect of particles size on tensile strength can be discribed through dislocation theory. The formation of plastic deformation needs to overcome the ultimate stress, which can attribute to a mass of moving dislocation. However, grain boundary will hinder the dislocation glide, and even leads to the dislocation pile-up. When the content of dislocation is pile-up increases a certain value, it will become the driving force of dislocation glide [37]. Furthermore, the particle size becomes larger, the content of dislocation pile-up is more; and the driving force of dislocation glide is bigger. That is why alloy with small particle size exhibits high strength. At the same time, due to small particle size increasing the number of particle boundary, the ability of hindering the dislocation motion is high. Therefore, the UTS for the plastic deformation is strongly influenced by Mg_2Si particles size.

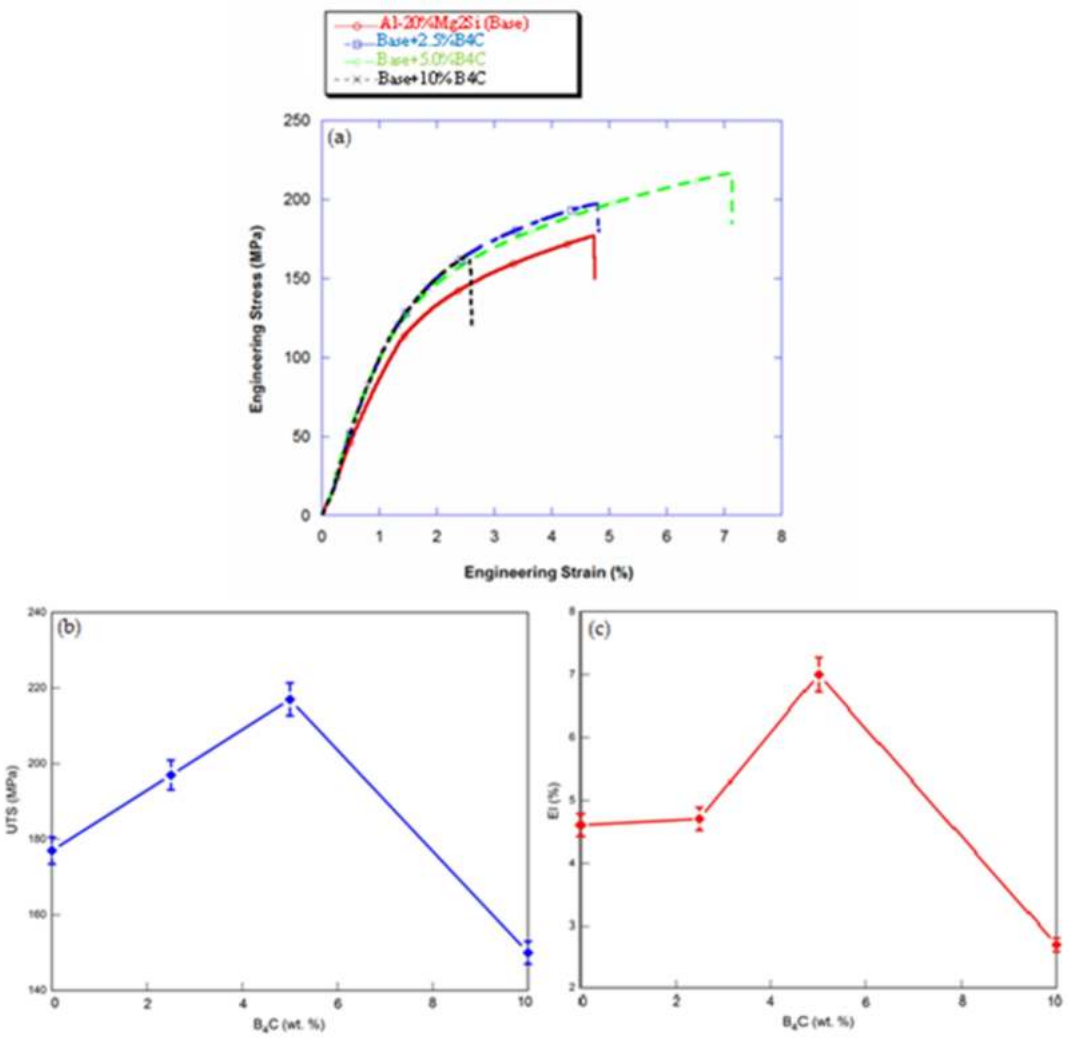

Figure 12. (**a**) Engineering stress-strain curve of Al-20%Mg_2Si with various content of B_4C (**b**) the ultimate tensile strength (UTS) and (**c**) percentage elongation (El%) values of Al-Mg_2Si composite with different B_4C contents.

However, as shown in Figure 12b,c, when the concentration of B_4C increased to 10 wt%, the UTS and El% of the composite reduced to 150 MPa and 2.7%, which is lower than other fabricated composites. The reduction in the tensile properties of the composite from the addition of higher B_4C concentration (10 wt%) is due to the agglomeration of B_4C particles as well as their non-uniform distribution in the matrix (Figure 3d). In fact, in the agglomerated areas, the bonding strength between the Al matrix and B_4C particles is low and the load transferring from the matrix to B_4C particles is not appropriate. Such insufficiencies cause a crack or decohesion of nucleation sites, which lead to composite failure at low stress levels. Furthermore, the addition of 10 wt% B_4C to Al-20%Mg_2Si composite results in increment in the average size of primary Mg_2Si particles (Figures 3 and 4), which leads to a decrease in the tensile properties. A bigger size of primary Mg_2Si provides more potential substrates for nucleation and propagation of a crack, resulting in the failure of the composite by particle fracture [38].

3.5.3. Fracture Surface

The SEM images of tensile fracture surfaces of the Al-20%Mg_2Si composite added with different percentages of B_4C are exhibited in Figure 13a–f. Primary Mg_2Si particle is intrinsically brittle and has more intrinsic defects, which cause cellular fracture mode in the fracture surface of base Al-20%Mg_2Si composite due to cleavage in fracture planes of coarse Mg_2Si particles that are indicated by arrows (Figure 3a). Furthermore, the sharp corners of the irregular primary Mg2Si particles in the base Al-Mg_2Si composite serve as stress concentration sites for crack initiation and propagation which results in fracture of these coarse particles (Figure 3b) [39].

However, after adding B_4C particles up to 5 wt% to the Al-20%Mg_2Si composite, the fracture mode changed from brittle in the base composite to ductile, as depicted in Figure 13c,d. An interesting result is achieved for Al-20%Mg_2Si-5%B_4C hybrid composite, in which the fracture surface contains decohered primary Mg_2Si particles and a more ductile area. The obtained result is because of the presence of partially refined primary Mg_2Si particles and also B_4C particles, which have uniform distribution and good bonding with the Al matrix. The matrix alloy can be reinforced with a uniform distribution of the particle due to the effective role of the particle-rich region in the prevention of crack propagation; however, a particle-poor region offers canals for the propagation of crack [40]. Due to the decreasing size and aspect ratio of Mg_2Si particles after the addition of 5 wt% B_4C particles (Figure 4), the Mg_2Si provides less potential areas for crack nucleation compared to the base composite, and hence crack initiation is hindered. Furthermore, as the bonding between B_4C particles with the matrix is good, fracturing almost occurs in the B_4C particles rather than in the particle-matrix interface. This is in accordance with the model proposed by Babout et al. [41] in simulation of the fracture behavior in MMCs. Based on their suggestion, regardless of particle density, the fracture of interface is strength controlled, and decohesion occurred once the tensile stress in the particles exceeded the interface strength as a critical value. Based on these results, it is concluded that the Al-B_4C interface is steady and stable, hence, the initiation and propagation of the cracks is from Mg_2Si particles and not the Al-B_4C interface. Moreover, as seen in Figure 13d, the fracture surface exhibits several dimples, which are indications of a ductile fracture. This result is aligned with high strength and elongation of composite, as shown in Figure 12.

Figure 13e,f depicts the fracture surface of Al-20%Mg_2Si-10%B_4C hybrid composite. As observed, B_4C particles agglomerate in some areas on the fracture surface. The particle agglomeration increases the local stresses and proffers substrates for nucleation of crack and low energy propagation canals across the linked brittle particles. Failure can be portrayed by higher stresses generated in these areas. The interface of B_4C/matrix where the B_4C particles agglomerate shows interfacial decohesion, in which the failure took place along this interface. If the bonding strength in the interface between particle and matrix is weak, debonding occurs between matrix and particles before a particle fracture [39]. As the B_4C particles debonded from the matrix in a brittle manner, this feature reveals a weak

interface bonding which creates favorable substrates for the initiation of crack and drops the load bearing capacity of the composite. In this condition, the crack needs less energy to propagate through the interface which can be reconciled with low strength and elongation of composite, as depicted in Figure 12. The crack initiates at the interface between particle and matrix, then propagates through the matrix, and finally joins other cracks, resulting in composite failure.

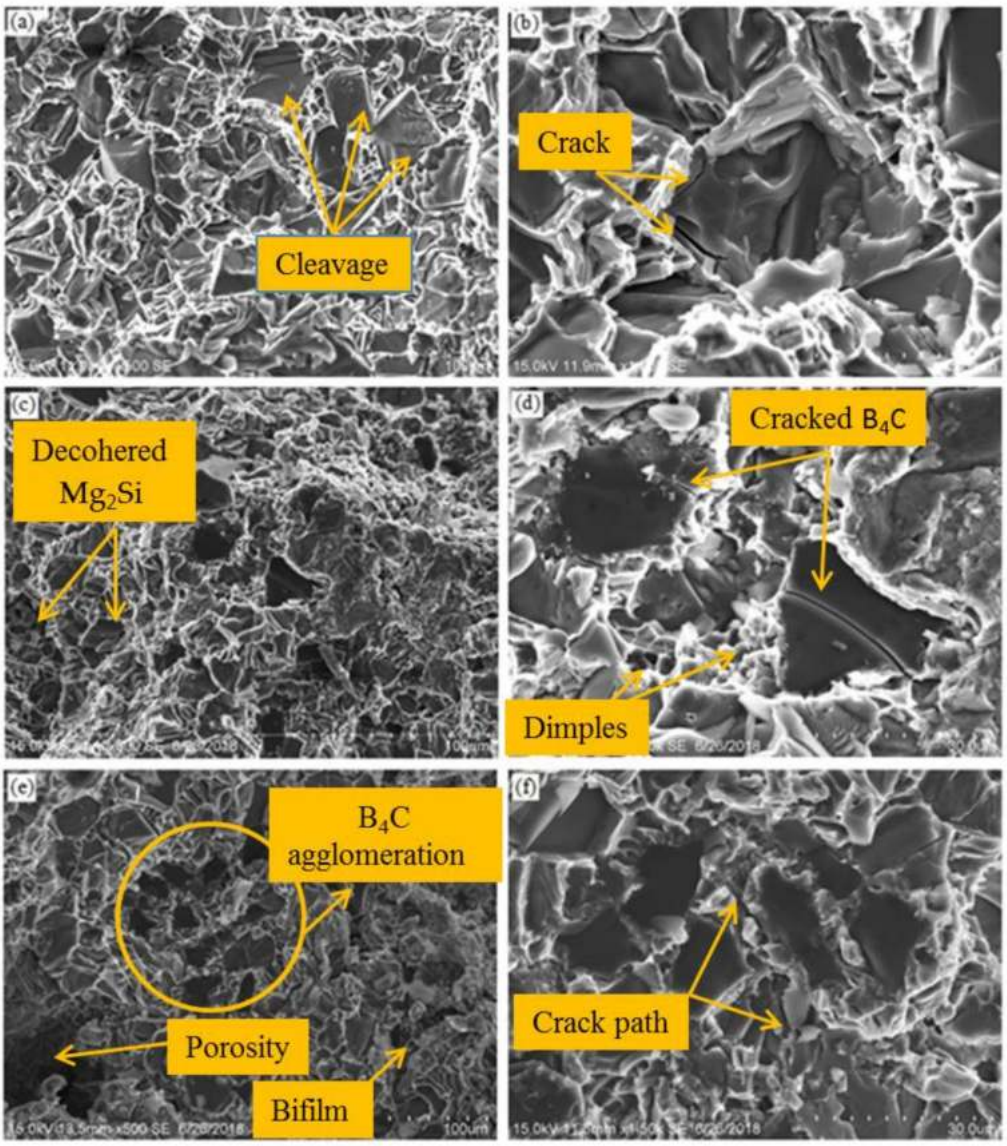

Figure 13. Fractography of Al-20%Mg_2Si tensile samples with different contents of B_4C in low (left) and high (right) magnifications: (**a**,**b**) 0, (**c**,**d**) 5, and (**e**,**f**) 10 wt% B_4C.

Porousity and bifilm on fracture surface are clearly observed in Figure 13e. It has been reported in many investigations that with increasing volume fraction of the reinforcement particles, internal defects, such as porousity and oxide layer (bifilm) expand [42]. During composite fabrication via vortex system and pouring of the molten metal matrix composite in the mould cavity, the bifilms or folded-over films are entrained, leading to successive impairing of UTS and El% of the composite (Figure 12). Not only does the unbounded oxide-oxide interface of the bifilms introduce stress concentration, the films also act as pre-existing microcracks.

3.6. Wear Behavior

Figure 14 demonstrates that the wear rate of Al-20%Mg_2Si composites correspond to different B_4C additions under the applied loads of 20 and 40 N. As seen, with the addition of 5 wt% B_4C, the wear resistance increased when the wear rate of Al-20%Mg_2Si composites decreased from 0.85 mm^3/km to 0.46 mm^3/km under 20N applied load. This improvement was the result of the load bearing capacity of the composites by ceramic particles during sliding. This was similar to the results reported by [43] in Mg-TiO_2 magnesium matrix composite, where, the addition of 5 wt% TiO_2 into the Mg matrix improved the wear resistance of the composite. The enhancement in wear resistance could be associated with the increase in hardness, in which the hardness of the Al-20%Mg_2Si composites with the addition of 5 wt% B_4C increased to 100 HV (Figure 11). The connection between hardness and wear rate can be explained by Archard's law, which describes an inverse proportionality between hardness and the wear rate of a material [44].

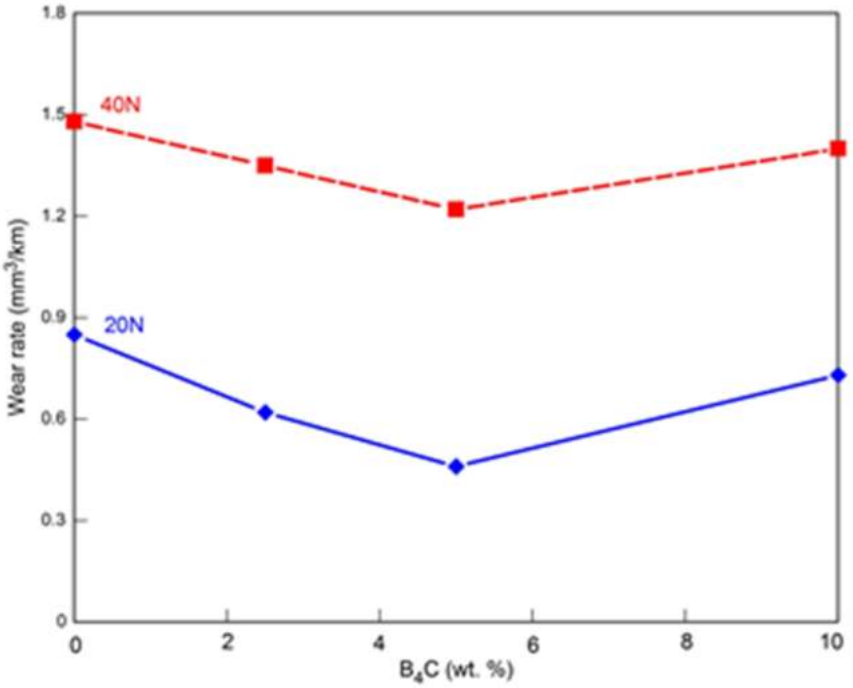

Figure 14. Wear rate of Al-Mg_2Si composite reinforced with different amount of B_4C particles under applied loads of 20 and 40 N.

Another reason for the decrease in the wear rate of the composite is due to the partial refinement of primary Mg_2Si particles, as shown in Figures 3 and 4. It was expected that during the wear test, the wear rate of the hybrid composite with a finer Mg_2Si size decreases because grain boundary strengthening occurs with smaller particle size, leading to strain hardening [45]. With the addition of 10 wt% B_4C to the Al-20%Mg_2Si composites, the wear resistant was supposed to increase; however, as seen in Figure 14, the wear rate increased to 0.73 mm^3/km, causing the increase in material removal. The high wear rate of Al-20%Mg_2Si-10%B_4C hybrid composite was due to the agglomeration of the B_4C particles in the matrix (Figure 3d), which resulted in the 'three-body' wear during sliding and increment of the composite's wear rate. Additionally, due to the fragile bonding between the matrix and B_4C in the agglomerated regions, the B_4C particles were unable to support the applied load efficiently. Therefore, the interface offered a site for crack nucleation and tended to pull out the particles from the wear surface, which led to the formation and propagation of crack in the subsurface wear region [46]. In addition, as mentioned before in Figure 4, increasing the content of B_4C to 10 wt%, decreased the density of primary Mg_2Si particles. As a result, the load bearing effect of the hybrid composite reduced and during

the wear rate the soft Al matrix was subjected to the asperities of the steel disc which led to an increase in the wear rate. Figure 14 also illustrates the increased wear rate when the applied load is increased from 20N to 40N. This is expected as the number of contact asperities and the separation of surface asperities increased at the higher loads. Increasing the applied load also contributed to the accumulation of wear debris in the space between the pin and disc that led to a more serious abrasive wear, increasing the wear rate.

The coefficient of friction (COF) of the Al-20%Mg_2Si composites added with various content of B_4C for the applied loads of 20 and 40 N is depicted in Figure 15. As seen, similar to the trend of wear rate, under the applied load of 20N, the COF (μ) of the Al-20%Mg_2Si composite decreased from 0.46 in the base Al-20%Mg_2Si composite to 0.43 and 0.39 when the composite was treated with 2.5 and 5 wt% B_4C respectively. Hence, Al-20%Mg_2Si-5%B_4C hybrid composite has the lowest COF compared to other fabricated composites. The reason for the reduction of the COF in the composite added with 5% B_4C can be related to the increased hardness of the composite (Figure 11) as finer Mg_2Si particles can support more load, and decrease the contact area between the pin and the sliding disc. This indirectly prevents the pin surface from acquiring more scratches. In addition, Devaraju, et al. [47] reported that the segregation of boron which acted as a dry lubricant between the sliding surfaces, leads to a decreased friction coefficient.

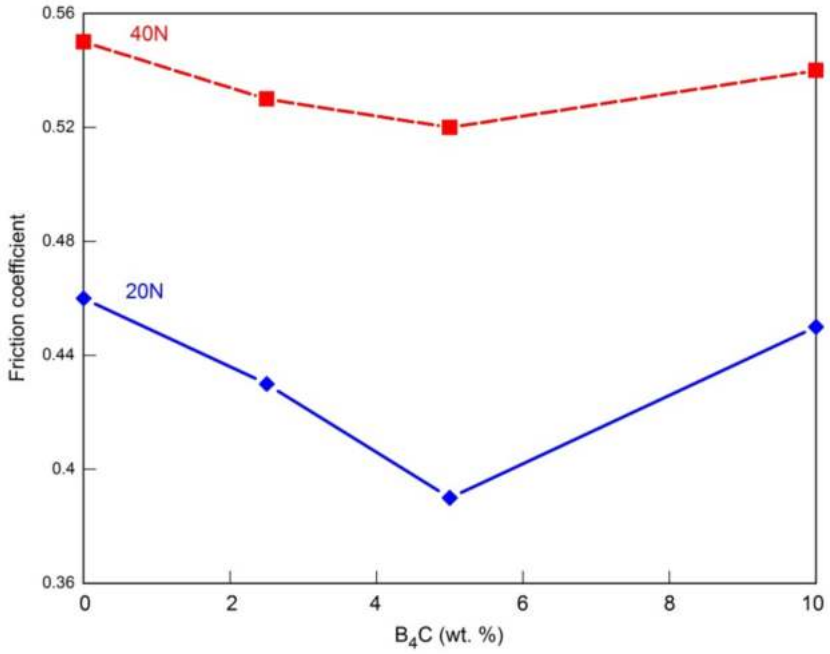

Figure 15. Coefficient of friction of Al-20%Mg_2Si composite reinforced with different amount of B_4C particles.

However, with a further increase in the B_4C content to 10%, the COF increases to 0.45. Due to the agglomeration of B_4C particles in 10 wt% B_4C hybrid composite, the minority of the Mg_2Si particles appeared in coarse size. The fracture of the large and brittle Mg_2Si could initiate the crack propagation in the matrix, and small Mg_2Si particles are pulled out from the matrix, which further acts as the source for abrasive wear, causing the COF to increase. The increasing COF could also is due to the fragmentation of boron oxide layer. B_2O_3 layer occurred when the pulled out B_4C particles reacted with the atmosphere. Its delamination during dry sliding formed scratches and grooves on the pin surface that increased the friction between the pin and the sliding surface [48].

An increase in the applied load to 40 N increases the COF of the composites compared to the 20 N applied load; however, the Al-20%Mg_2Si composite added with 5 wt% B_4C owns the lowes COF (0.52) compared to other fabricated composites and addition of 10 wt%

B_4C incresed the COF to 0.54, which is similar with the trend of COF of the composites under 20N.

Figure 16a–f demonstrates the worn surface of the fabricated composites added with 0, 5, and 10 wt% B_4C particles under the applied loads of 20 and 40 N. The worn surface of Al-Mg_2Si composite (Figure 16a) displays several continuous grooves parallel to the sliding direction. Moreover, the counterfaces between the pin and the sample surface increased; hence, more materials were detached from the sample's surface. This detachment may be due to the adhesive friction that subsequently increased the wear rate (Figure 14). The principal wear mechanisms of the samples were abrasion and delamination wear. By increasing the load to 40 N, delamination and adhesion govern the wear mechanisms, in which extensive pits and large size of delamination flakes exist on the worn surface, indicating the alteration of wear mechanism to severe wear (Figure 16b). With the addition of 5 wt% B_4C particles to the Al-20%Mg_2Si composite, the delamination pit areas as well as the groove width decreased, illustrating a mild abrasive wear mechanism, as shown in Figure 16c. This is consistent with decreasing wear rate and coefficient of friction results depicted in Figures 14 and 15, respectively.

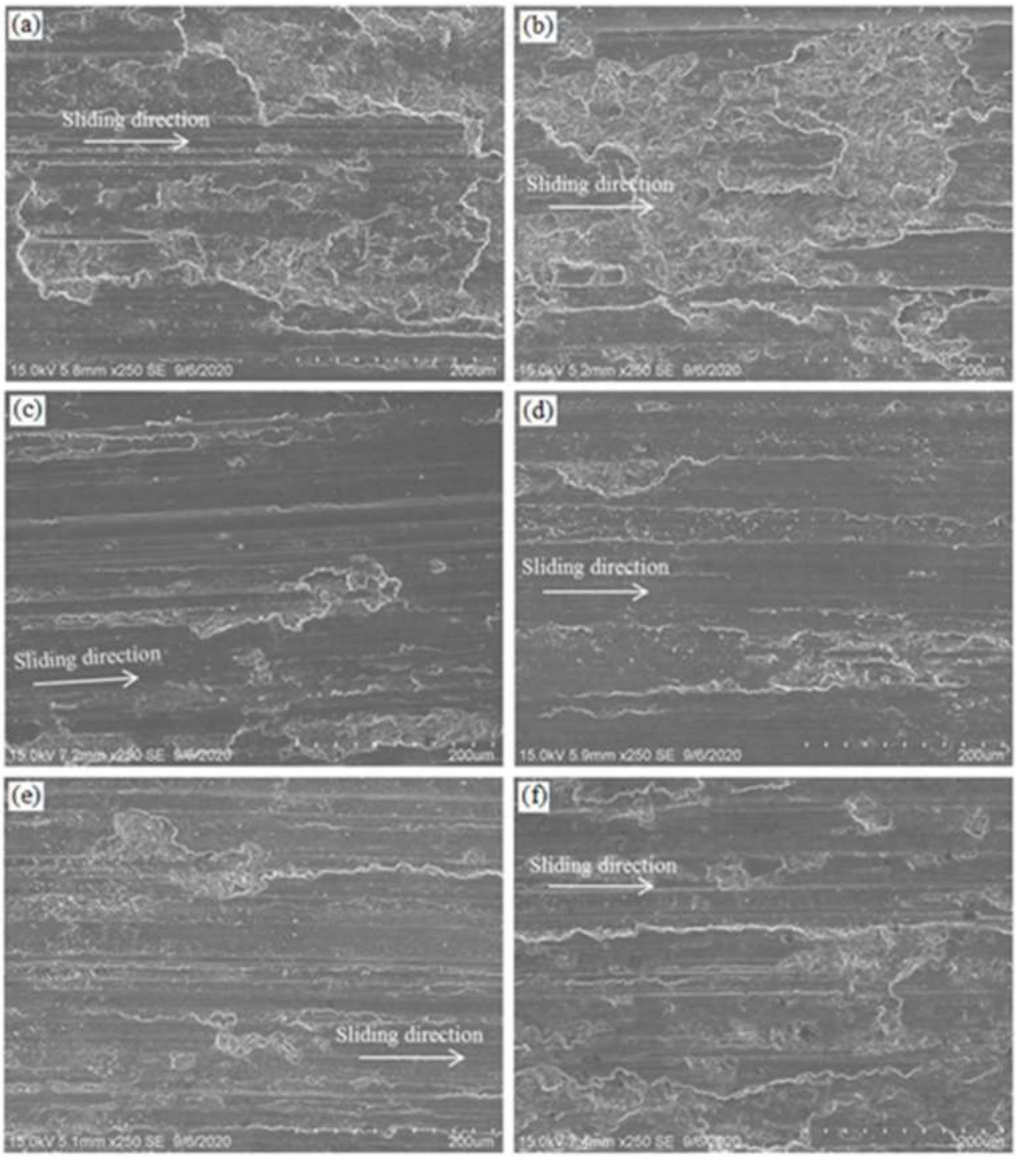

Figure 16. SEM micrographs of the worn surface of Al-Mg_2Si composite samples with various B_4C contents (**a**,**b**) 0 wt%, (**c**,**d**) 5 wt%, and (**e**,**f**) 10 wt% under 20 N (left) and 40 N (right) applied loads.

On the other hand, as observed in Figure 16e, by adding 10 wt% B_4C to the Al-20%Mg_2Si composite, deep parallel grooves with large widths indicate a severe abrasion, which is regularly produced by rigid particles between the pin and disc that cut into the worn surface. As observed in Figure 3d, the introduction of a high percentage of B_4C particles (10 wt%) to the Al-20%Mg_2Si composite caused the B_4C particles to cluster in some regions in the matrix with a non-uniform distribution. Therefore, during the sliding wear test, the agglomerated B_4C particles were pulled out from the matrix, fragmented, and became entrapped between the pin and disc. As a result, abrasion took place, leading the material to be omitted from the abrasion groove Figure 16e. Hence, the predominant wear mechanisms were severe abrasion and delamination. In addition, by increasing the applied load to 40 N, the flake-like delamination pit areas as well as abrasion grooves become wider and deeper, as seen in Figure 16f. This extensive delamination is due to crack nucleation and propagation sourced from the fracture and detachment of B_4C particles.

4. Conclusions

The effects of various B_4C additions on the microstructural, mechanical, and tribological properties of Al-20%Mg_2Si composite were investigated. It can be concluded that:

1. With the addition of 5 wt% B_4C, the mean size of primary Mg_2Si in Al-20%Mg_2Si composite decreased from 47 to 33 μm, and its morphology was altered from octahedral to polygonal shape. However, with further addition of B_4C to 10 wt%, the morphology of primary Mg_2Si remains in polygonal shape with an increase in its size to 38 μm.
2. The tensile result showed that the best level of B_4C was 5 wt% in which the UTS and El.% of Al-20%Mg_2Si composite increased from 177 MPa and 4.6% to 217 MPa and 7% in the Al-20%Mg_2Si-5%B_4C hybrid composite, respectively. The mechanisms of strengthening of the composites were load transfer effects, dislocation strengthening, and grain refinement. In addition, the Vickers hardness value of Al-20%Mg_2Si composite increased from 75 Hv to 100 Hv after the addition of 5 wt% B_4C particles to the composite.
3. Examination of the fracture surface revealed that the fracture of the Al-20%Mg_2Si composite was brittle (including the cleavages). With the addition of 5 wt% B_4C particles, the fracture surface owned more dimples, which represents the domination of the ductile fracture.
4. The results of the sliding wear test showed that the addition of 5 wt% B_4C to the Al-20%Mg_2Si composite improved the wear resistance of the alloy by decreasing the wear rate by 46%. The enhancement in wear resistance was due to the self-lubrication function of B_4C, uniform distribution of B_4C particles and good bonding of B_4C with the matrix as well as the small size of primary Mg_2Si particles, which in turn decreased the friction coefficient of the composite.
5. Examination on the worn surface revealed that the governed wear mechanisms of the Al-20%Mg_2Si composite were abrasion and delamination, which changed to mid abrasion in the Al-20%Mg_2Si-5%B_4C hybrid composite.

Author Contributions: H.G., M.A.J., and A.B. methodology, formal analysis, investigation, writing—original draft; H.G., K.K., and S.S.R.K. conceptualization, methodology, software, formal analysis, investigation, writing—original draft; T.A.A.B., K.K., and M.P. validation, resources, supervision, writing—review & editing. All authors have read and agreed to the published version of the manuscript.

Funding: This research is financially supported by Universiti Teknologi Malaysia (UTM) under the research grants 04E95 and 06G22. In addition, this research was supported by the Ministry of Education, Youth, and Sports of the Czech Republic and the European Union (European Structural and Investment Funds Operational Program Research, Development, and Education) in the framework of the project "Modular platform for autonomous chassis of specialized electric vehicles for freight and equipment transportation", reg. no. CZ.02.1.01/0.0/0.0/16_025/0007293.

Institutional Review Board Statement: Not applicable.

Informed Consent Statement: Not applicable.

Data Availability Statement: Not applicable.

Acknowledgments: The authors acknowledge Universiti Teknolgi Malaysia (UTM) for provision of research facility.

Conflicts of Interest: The authors declare that they have no known competing financial interests or personal relationships that could have appeared to influence the work reported in this paper.

References

1. Srivastava, A.; Dixit, A.; Tiwari, S. A Review on Fabrication and Characterization of Aluminium Metal Matrix Composite (AMMC). *Int. J. Adv.* **2014**, *2*, 516–521.
2. Lu, L.; Lai, M.O.; Hoe, M.L. Format on of nanocrystalline Mg_2Si and Mg_2Si dispersion strengthened Mg-Al alloy by mechanical alloying. *Nanostruct. Mater.* **1998**, *10*, 551–563. [CrossRef]
3. Bonnet, G.; Rohr, V.; Chen, X.-G.; Bernier, J.-L.; Chiocca, R.; Issard, H. Use of Alcan's Al-B_4C metal matrix composites as neutron absorber material in TN International's transportation and storage casks, Packaging, Transport. *Storage Secur. Radioact. Mater.* **2009**, *20*, 98–102. [CrossRef]
4. Pozdniakov, A.; Zolotorevskiy, V.; Barkov, R.; Lotfy, A.; Bazlov, A. Microstructure and material characterization of 6063/B_4C and 1545K/B_4C composites produced by two stir casting techniques for nuclear applications. *J. Alloy. Compd.* **2016**, *664*, 317–320. [CrossRef]
5. McClellan, K.J.; Chu, F.; Roper, J.M.; Shindo, I. Room temperature single crystal elastic constants of boron carbide. *J. Mater. Sci.* **2001**, *36*, 3403–3407. [CrossRef]
6. Dodd, S.P.; Saunders, G.A.; James, B. Temperature and pressure dependences of the elastic properties of ceramic boron carbide (B4C). *J. Mater. Sci.* **2002**, *37*, 2731–2736. [CrossRef]
7. Pozdniakov, A.; Lotfy, A.; Qadir, A.; Shalaby, E.; Khomutov, M.; Churyumov, A.; Zolotorevskiy, V. Development of Al-5Cu/B_4C composites with low coefficient of thermal expansion for automotive application. *Mater. Sci. Eng. A* **2017**, *688*, 1–8. [CrossRef]
8. Canakci, A.; Arslan, F.; Varol, T. Effect of volume fraction and size of B_4C particles on production and microstructure properties of B_4C reinforced aluminium alloy composites. *Mater. Sci. Technol.* **2013**, *29*, 954–960. [CrossRef]
9. Baradeswaran, A.; Perumal, A.E. Perumal, Influence of B_4C on the tribological and mechanical properties of Al 7075-B_4C composites. *Compos. Part B* **2013**, *54*, 146–152. [CrossRef]
10. Lashgari, H.; Zangeneh, S.; Shahmir, H.; Saghafi, M.; Emamy, M. Heat treatment effect on the microstructure, tensile properties and dry sliding wear behavior of A356-10%B_4C cast composites. *Mater. Des.* **2010**, *31*, 4414–4422. [CrossRef]
11. Gudipudi, S.; Nagamuthu, S.; Subbian, K.S.; Prakasa, S.; Chilakalapalli, R. Enhanced mechanical properties of AA6061-B_4C composites developed by a novel ultra-sonic assisted stir casting. *Eng. Sci. Technol. Int. J.* **2020**, *23*, 1233–1243. [CrossRef]
12. Patidar, D.; Rana, R. Effect of B_4C particle reinforcement on the various properties of aluminium matrix composites: A survey paper. *Mater. Today Proc.* **2017**, *4*, 2981–2988. [CrossRef]
13. Moktar, M.S.; Ghandvar, H.; Abu Bakar, T. Microstructural and tensile properties of Al-20%Mg_2Si-xSiCp hybrid metal matrix composite. *Encycl. Renew. Sustain. Mater.* **2020**, *5*, 54–63. [CrossRef]
14. Sukiman, N.A.; Ghandvar, H.; Abu Bakar, T.; Wee, Y.C. Microstructure characterization and tensile properties of Al-15%Mg_2Si-xYSZ hybrid composite. *Malays. J. Microsc.* **2019**, *15*, 30–37.
15. Uvaraja, V.C.; Natarajan, N. Tribological characterization of stir-cast hybrid composite Aluminium 6061 reinforced with SiC and B_4C particulates. *Eur. J. Sci. Res.* **2012**, *76*, 539–552.
16. Aziz, M.A.; Mahmoud, T.S.; Zaki, Z.I.; Gaafer, A.M. Heat treatment and wear characteristics of Al_2O_3 and tic particulate reinforced AA6063 alloy hybrid composites. *J. Tribol.* **2006**, *128*, 891–904. [CrossRef]
17. Benal, M.M.; Shivanand, H.K. Effects of reinforcement content and ageing durations on wear characteristics of Al6061 based hybrid composites. *Wear* **2007**, *262*, 759–763. [CrossRef]
18. Umanath, K.; Selvamani, S.T.; Palanikumar, K. Friction and wear behaviour of Al6061 alloy (SiCp+ Al_2O_3) hybrid composites. *Int. J. Eng. Sci. Technol.* **2011**, *3*, 5441–5451.
19. Altinkok, N.; Coban, A. The tensile behaviour and microstructure of Al_2O_3/SiCp reinforced aluminium-based mmcs produced by the stir casting method. *Int. J. Adv. Sci. Technol.* **2012**, *2*, 78–86.
20. Uvaraja, V.C.; Natarajan, N.; Rajendran, I.; Sivakumar, K. Tribological behaviour of novel hybrid composite materials using Taguchi technique. *J. Tribol.* **2013**, *135*, 021101. [CrossRef]
21. Sharma, S.S.; Jagannath, K.; Prabhu, P.R.; Gowri, S.; Harisha, S.R.; Kini, U.A. Metallography & bulk hardness of artificially aged Al6061-B_4C-sic stir cast hybrid composites. *Mater. Sci. Forum.* **2017**, *880*, 140–143. [CrossRef]
22. Uthayakumar, M.; Aravindan, S.; Rajkumar, K. Wear performance of Al-SiC-B_4C hybrid composites under dry sliding conditions. *Mater. Design.* **2013**, *47*, 456–464. [CrossRef]
23. Lin, Q.; Shen, P.; Qiu, F.; Zhang, D.; Jiang, Q. Wetting of polycrystalline B4C by molten Al at 1173–1473K. *Scr. Mater.* **2009**, *60*, 960–963. [CrossRef]

24. Wu, H.; Zeng, F.; Yuan, T.; Zhang, F.; Xiong, X. Wettability of 2519Al on B4C at 1000–1250 °C and mechanical properties of infiltrated B4C-2519Al composites. *Ceram. Int.* **2014**, *40*, 2073–2081. [CrossRef]
25. Shirvanimoghaddam, K.; Khayyam, H.; Abdizadeh, H.; Karbalaei, A.M.; Pakseresht, A.H.; Ghasali, E.; Naebe, M. Boron carbide reinforced aluminium matrix composite: Physical, mechanical characterization and mathematical modelling. *Mater. Sci. Eng. A* **2016**, *658*, 135–149. [CrossRef]
26. Harichandran, R.; Selvakumar, N. Effect of nano/micro B_4C particles on the mechanical properties of aluminium metal matrix composites fabricated by ultrasonic cavitation-assisted solidification process. *Arch. Civ. Mech. Eng.* **2015**, *16*, 147–158. [CrossRef]
27. Mehmet, I.; Amin, N.; Onder, A.; Sabri, A. Mechanical characterization of B_4C reinforced aluminum matrix composites produced by squeeze casting. *Mater. Res. Soc.* **2016**, *32*, 1–7. [CrossRef]
28. Hashim, J.; Looney, L.; Hashmi, M.S.J. Metal matrix composites: Production by the stir casting method. *J. Mater. Process. Technol* **1999**, *92*, 1–7. [CrossRef]
29. Bramfitt, B.L. The effect of carbide and nitride additions on the heterogeneous nucleation behavior of liquid iron. *Metall. Trans.* **1970**, *1*, 197–201. [CrossRef]
30. Shabestari, S.G.; Malekan, M. Assessment of the effect of grain refinement on the solidification characteristics of 319 aluminum alloy using thermal analysis. *J. Alloys. Compd.* **2010**, *492*, 134–142. [CrossRef]
31. Ghandvar, H.; Idris, M.H.; Ahmad, N.; Emamy, M. Effect of gadolinium addition on microstructural evolution and solidification characteristics of Al-15%Mg_2Si in-situ composite. *Mater. Char.* **2018**, *135*, 57–70. [CrossRef]
32. Nagarajan, S.; Dutta, B.; Surrapa, M.K. The effect of SiC particles on the size and morphology of eutectic silicon in cast A356/SiCp composites. *Compos. Sci. Technol.* **1999**, *59*, 897–902. [CrossRef]
33. Li, Y.Z.; Wang, Q.Z.; Wang, W.G.; Xiao, B.L.; Ma, Z.Y. Interfacial reaction mechanism between matrix and reinforcement in B_4C/6061Al composites. *Mater. Chem. Phys.* **2015**, 1–11. [CrossRef]
34. Azarbarmas, M.; Emamy, M.; Karamouz, M.; Alipour, M.; Rassizadehghani, J. The effects of boron additions on the microstructure, hardness and tensile properties of in situ Al-15%Mg_2Si composite. *Mater. Design.* **2011**, *32*, 5049–5054. [CrossRef]
35. Viala, J.C.; Bouix, J.; Gonzalez, G.; Esnouf, C. Chemical reactivity of aluminium with boron carbide. *J. Mater. Sci.* **1997**, *32*, 4559–4573. [CrossRef]
36. Lashgari, H.R.; Emamy, M.; Razaghian, A.; Najimi, A.A. The effect of strontium on the microstructure, porosity and tensile properties of A356-10%B_4C cast composite. *Mater. Sci. Eng. A* **2009**, *517*, 170–179. [CrossRef]
37. Ghandvar, H.; Farahany, S.; Idris, J. Wettability Enhancement of SiCp in Cast A356/SiCp Composite Using Semisolid Process. *Mater. Manuf. Process.* **2015**, *30*, 1442–1449. [CrossRef]
38. Song, M. Effects of volume fraction of SiC particles on mechanical properties of SiC/Al composites. *Trans. Nonferrous Metals Soc. China* **2009**, *19*, 1400–1404. [CrossRef]
39. Qi, G.; Shusen, W.; Shulin, L.; Xuecheng, D.; Zhiyuan, Z. Preparation of in- situ TiB_2 and Mg_2Si hybrid particulates reinforced Al-matrix composites. *J. Alloy. Compd.* **2015**, *651*, 521–527. [CrossRef]
40. Moses, J.; Dinaharan, I.; Sekhar, S. Prediction of influence of process parameters on tensile strength of AA6061/TiC aluminum matrix composites produced using stir casting. *Trans. Nonferrous Met. Soc. China* **2015**, *26*, 1498–1511. [CrossRef]
41. Babout, L.; Maire, E.; Buffière, J.Y.; Fougères, R. Characterization by X-ray computed tomography of decohesion, porosity growth and coalescence in model metal matrix composites. *Acta Mater.* **2001**, *49*, 2055–2063. [CrossRef]
42. Mohammadi, H.; Emamy, M.; Hamnabard, Z. The statistical analysis of tensile and compression properties of the as-cast AZ91-X%B_4C composites. *Inter. Metal. Cast.* **2020**, *14*, 505–517. [CrossRef]
43. Lakshmanan, P.A. Fabrication and Tribological Behaviour of (Mg-TiO_2) Composites. *Trans. Famena* **2017**, *41*, 61–70. [CrossRef]
44. Archard, J. Contact and rubbing of flat surfaces. *J. Appl. Phys.* **1953**, *24*, 981–988. [CrossRef]
45. Thakur, S.K.; Dhindaw, B.K. The influence of interfacial characteristics between SiCp and Mg/Al metal matrix on wear, coefficient of friction and microhardness. *Wear* **2001**, *247*, 191. [CrossRef]
46. Basavarajappa, S.; Chandramohan, G.; Mukund, K.; Ashwin, M.; Prabu, M. Dry sliding wear behavior of Al 2219/SiCp-Gr hybrid metal matrix composites. *J. Mater. Eng. Perform.* **2006**, *15*, 668. [CrossRef]
47. Devaraju, A.; Pazhanivel, K. Evaluation of Microstructure, Mechanical and Wear Properties of Aluminium Reinforced with Boron Carbide Nano Composite. *Indian. J. Sci. Technol.* **2016**, *9*, 1–6. [CrossRef]
48. Tang, F.; Wu, X.; Ge, S.; Ye, J.; Zhu, H.; Hagiwara, M.; Schoenung, J. Dry sliding friction and wear properties of B_4C particulate-reinforced Al-5083 matrix composites. *Wear* **2008**, *264*, 555–561. [CrossRef]